

Evidence of abrupt changes in Western Mediterranean Deep Water circulation during the last 50 kyr: A high-resolution marine record from the Balearic Sea

J. Frigola^a, A. Moreno^b, I. Cacho^a, M. Canals^{a,*}, F.J. Sierro^c, J.A. Flores^c, J.O. Grimalt^d

^a*CRG Marine Geosciences, Department of Stratigraphy, Paleontology and Marine Geosciences, Faculty of Geology, University of Barcelona, Campus de Pedralbes, C/Martí i Franquès s/n, 08028 Barcelona, Spain*

^b*Pyrenean Institute of Ecology, Consejo Superior de Investigaciones Científicas, Apto. 202, 50080 Zaragoza, Spain*

^c*Department of Geology, University of Salamanca, Plaza de la Merced s/n, 37008 Salamanca, Spain*

^d*Department of Environmental Chemistry, Institute of Chemical and Environmental Research, Consejo Superior de Investigaciones Científicas, C/Jordi Girona 18, 08034 Barcelona, Spain*

Available online 27 June 2007

Abstract

The IMAGES core MD99-2343, recovered from a sediment drift north of the island of Minorca, in the north-western Mediterranean Sea, holds a high-resolution sequence that is perfectly suited to study the oscillations of the overturning system of the Western Mediterranean Deep Water (WMDW). Detailed analysis of grain-size and bulk geochemical composition reveals the sensitivity of this region to climate changes at both orbital and centennial–millennial temporal scales during the last 50 kyr. The dominant orbital pattern in the K/Al record indicates that sediment supply to the basin was controlled by the insolation evolution at 40°N, which forced changes in the fluvial regime, with more efficient sediment transport during insolation maxima. This orbital control also modulated the long-term pattern of the WMDW intensity as illustrated by the silt/clay ratio.

However, deep convection was particularly sensitive to climatic changes at shorter time-scales, i.e. to centennial–millennial glacial and Holocene oscillations that are well documented by all the paleocurrent intensity proxies (Si/Al, Ti/Al and silt/clay ratios). Benthic isotopic records ($\delta^{13}\text{C}$ and $\delta^{18}\text{O}$) show a Dansgaard–Oeschger (D–O) pattern of variability of WMDW properties, which can be associated with changing intensities of the deep currents system. The most prominent reduction on the WMDW overturning was caused by the post-glacial sea level rise.

Three main scenarios of WMDW overturning are revealed: a strong mode during D–O Stadials, a weak mode during D–O Interstadials and an intermediate mode during cooling transitions. In addition, D–O Stadials associated with Heinrich events (HEs) have a very distinct signature as the strong mode of circulation, typical for the other D–O Stadials, was never reached during HE due to the surface freshening induced by the inflowing polar waters. Consequently, the WMDW overturning system oscillated around the intermediate mode of circulation during HE. Though surface conditions were more stable during the Holocene, the WMDW overturning cell still reacted synchronously to short-lived events, as shown by increments in the planktonic $\delta^{18}\text{O}$ record, triggering quick reinforcements of the deep water circulation. Overall, these results highlight the sensitivity of the WMDW to rapid climate change which in the recent past were likely induced by oceanographic and atmospheric reorganizations in the North Atlantic region.

© 2007 Elsevier Ltd and INQUA. All rights reserved.

1. Introduction

Abrupt climate changes of different intensity and scales characterize the climate history of the last 50 kyr in the North Atlantic region. During the last glacial period a

series of coolings (Stadials) and warmings (Interstadials) known as the Dansgaard–Oeschger (D–O) events punctuated the Marine Isotopic Stage (MIS) 3 (Bond et al., 1993; Dansgaard et al., 1993). Additionally, abrupt coolings (known as Heinrich events, HEs) at the end of sequences of progressively weaker D–O oscillations resulted in massive iceberg discharges accompanied by deposition of ice rafted debris (IRD) (Heinrich, 1988; Bond et al., 1993). Climatic

*Corresponding author.

E-mail address: miquelcanals@ub.edu (M. Canals).

models suggest that reorganizations of the thermohaline circulation (THC) due to changes in the sea surface freshwater balance were the cause for the observed abrupt climate changes (Stocker, 2000). Similarly, the occurrence of abrupt climate changes during the Holocene at similar time-scales than those from the glacial period has been inferred from marine and terrestrial studies worldwide (Mayewski et al., 2004).

The rapid transmission of millennial-scale climate variability from the North Atlantic towards the Mediterranean region is supported by a number of studies (Rohling et al., 1998; Allen et al., 1999; Cacho et al., 1999, 2000, 2001; Combourieu Nebout et al., 2002; Moreno et al., 2002, 2004; Bartov et al., 2003; Martrat et al., 2004; Sierro et al., 2005). Both oceanic and atmospheric processes were proposed as forcing mechanisms for the climatic teleconnections between high and medium latitudes. However, an improved understanding on their effects over terrestrial and marine environments is still required. Recently, it has been demonstrated that the western Mediterranean overturning system was enhanced during collapse or reduction of the formation of North Atlantic Deep Water (NADW), likely favoured by the intensification of north-westerly winds as a consequence of the expansion of ice sheets in the North Atlantic region (Cacho et al., 2000; Moreno et al., 2002; Sierro et al., 2005). However, invasion of low-salinity waters from polar sources, including the melting of the icebergs released during the collapse of the NADW circulation at HEs, likely resulted in a temporary reduction of the formation of Western Mediterranean Deep Water (WMDW) (Sierro et al., 2005). In addition, changes in the properties and, possibly, in the volume of WMDW formed in the Gulf of Lion likely caused important modifications in the heat and salt volumes injected by the Mediterranean outflow water (MOW) into the North Atlantic, thus preconditioning the North Atlantic THC to switch from one mode to another (Bigg and Wadley, 2001; Voelker et al., 2006). The finding that a strong and dense MOW flowed at deeper levels during the Last Glacial Maximum than today (Rogerson et al., 2006) supports the view that the properties of the WMDW changed along the last deglaciation. Cacho et al. (2006) have reported changes in the deep-water temperature of WMDW related to the D–O cycles in core MD95-2043 from the Alboran Sea. Though on a very different time-scale, monitoring studies have revealed that WMDW density increased after the severe 2004/2005 winter in the north-western Mediterranean region (López-Jurado et al., 2005; Canals et al., 2006). From the above it becomes clear that both the influence of North Atlantic climate variability on WMDW formation and, inversely, the impact of Mediterranean Deep Waters on NADW production must be better understood as they are one of the key components of climate change during the last glacial period and the present interglacial in the concerned regions.

At present, the north/south displacements of the Azores high-Icelandic low-pressure system and their intensity

variations control the transmission of heat and moisture between low and high latitudes (Barry and Chorley, 1998; Bolle, 2003). This pattern is known as the North Atlantic Oscillation (NAO), which oscillates at decadal scale modulating much of the present-day climate variability in the entire region (Hurrell, 1995; Rodó et al., 1997). During a positive phase of the NAO, an increased pressure gradient in the North Atlantic region results in more frequent and stronger winter storms following a more northerly track, resulting in warm and wet winters in northern Europe. During a negative phase of the NAO, a reduced pressure gradient results in a southward displacement of the winter storms bringing higher precipitation to the Mediterranean region.

In this work, the analysis and interpretation of combined sedimentological proxies, i.e. grain-size parameters, and bulk geochemical ratios, together with the isotopic signal from planktonic and benthic foraminifera from core MD99-2343, allow the identification of changes in deep water properties and behaviour in the western Mediterranean Basin during the last 50 kyr. The results achieved so far provide new clues for understanding the mechanisms behind and the feedbacks of abrupt climate changes in the western Mediterranean region and their transmission to the deepest part of the western Mediterranean Basin.

2. Core location and present conditions

The present work focuses on the study of the 32.44 m long IMAGES-V core MD99-2343 recovered north of the Minorca Island (40°29.84'N, 04°01.69'E) at 2391 m of water depth, onboard R/V *Marion Dufresne* (Fig. 1). The core was recovered in a sediment drift formed by deep contour currents belonging to the southward branch of the WMDW flow, which borders the Valencia Trough from north to south following a cyclonic pattern at depths of ~2000 m (Millot, 1999) (Fig. 1). At this place the abrupt slope of the Balearic Promontory opposes deep circulation that accelerates and turns eastward bordering the base-of-slope of Minorca in its way to the open basin. Although no current meter data have been collected at the core location, intense deep currents have been interpreted from seafloor bedforms (Mauffret et al., 1982; Maldonado et al., 1985a; Palanques et al., 1995). Additionally, the base-of-slope peripheral depression and the associated sediment drift, previously described by Velasco et al. (1996), demonstrate the existence of relatively intense deep currents sweeping the deep slope north of Minorca.

The formation of a sediment drift is also depending on sediment availability. Most sediment inputs to this region come from the Ebro and Rhône fluvial discharges. However, only 10% of this sediment discharge reaches the deep basin (Martin et al., 1989) and the core location is too far from the coast to directly receive material from riverine origin. In the specific setting of the Balearic margin local mass gravity flows and hemipelagic settling have been identified as significant contributors of sediment to the

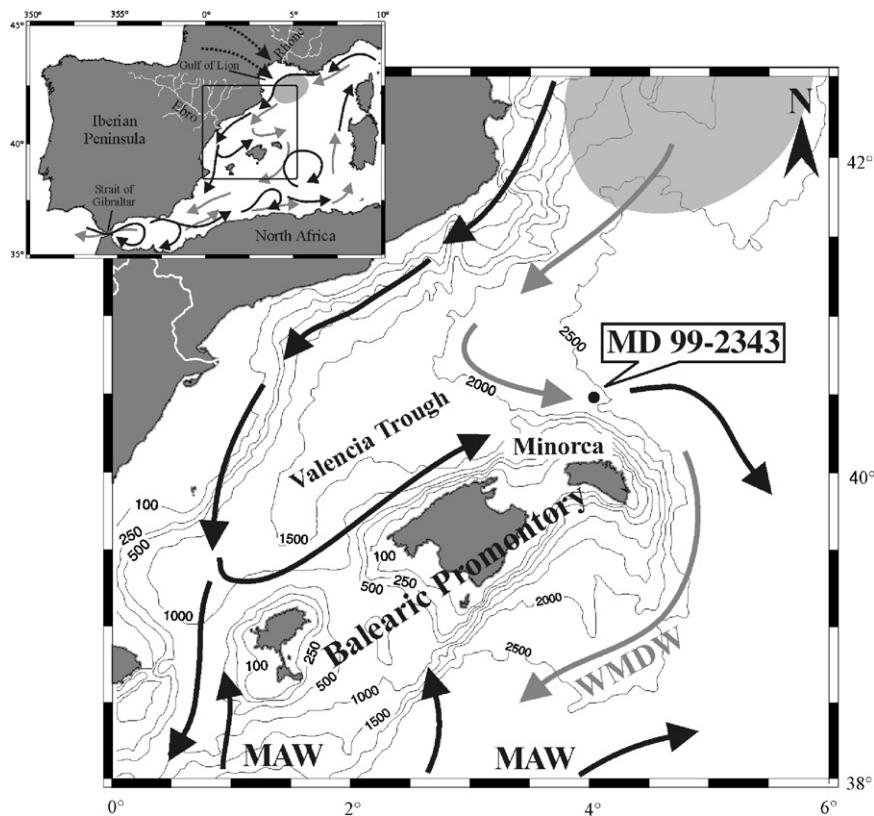


Fig. 1. Bathymetric map of the study area in the north-western Mediterranean Basin showing the location of core MD99-2343. Surface and deep main circulation patterns are represented by black and gray arrows, respectively. The shaded area shows the region of WMDW formation in the Gulf of Lion under the influence of north-westerly winds, illustrated as dotted arrows (inset). Rhône and Ebro Rivers supplying most freshwater inputs to this basin are also shown.

deep margin and basins surrounding the promontory (Maldonado et al., 1985a,b; Nelson and Maldonado, 1990; Alonso et al., 1995; Palanques et al., 1995; Calafat et al., 1996). Subsequently, deep water currents are assumed to rework, sort and transport these sediments and accumulate specific fractions on the sediment drift where core MD99-2343 was recovered (Fig. 1).

This Minorca sediment drift has been built under the action of deep contour currents related to the WMDW, which to a large extent forms in the Gulf of Lion by evaporation and cooling of the sea surface mostly during cold and windy winters, thus increasing the density of offshore surface waters until they sink (MEDOC, 1970; Lacombe et al., 1985; Millot, 1999). In addition to offshore convection, episodic dense shelf water cascading in the Gulf of Lion has been recently described to account for large volumes of sinking waters that add to WMDW (Canals et al., 2006). Deep water sources in the Gulf of Lion depend on wind stress variability and fluvial water discharge on the shelf preconditioning buoyancy. The formation of WMDW is also affected by the amount and depth of the warm and salty Levantine Intermediate Water (LIW) available in the basin before each event (Pinaridi and Masetti, 2000; Millot and Taupier-Letage, 2005). LIW forms in the eastern Mediterranean basin as a consequence

of evaporation and sinking of Modified Atlantic Water (MAW), which entered the Mediterranean Sea across the Strait of Gibraltar due to the negative hydrological balance caused by the excess of evaporation over freshwater inputs (Millot, 1999). At the end of a general cyclonic pattern, the dense LIW and WMDW leave the Mediterranean Basin through the Strait of Gibraltar as the deep MOW (Millot, 1999).

3. Material and methods

3.1. MD99-2343 core description

This study focuses on the top 17 m of the core that corresponds to the last 50 kyr (see Section 3.4 below). The upper 5 m (deglaciation and Holocene) consists of homogeneous gray nannofossil and foraminifer silty clay with moderate bioturbation. Below the top 5 m (last glacial period) the sediments are much more laminated and present mm to cm-thick grayish orange, yellowish brown, light olive brown and brownish black layers within a dominant homogeneous gray silty clay. Rare sandy layers were also described onboard. Moderate bioturbation, pyrite, organic matter, foram-rich and broken-shell layers were also observed throughout this section. Onboard

smear slides showed high contents of detrital minerals with abundant quartz and mica silt grains.

One centimeter thick samples were taken every 4–6 cm for grain-size and major element composition analyses of the bulk sediment. In addition, samples every 2 cm were taken for grain-size analyses along specific intervals.

3.2. Geochemical analyses

The content of major elements in sediment samples was determined by means of X-ray fluorescence using a PW 2400 sequential wavelength disperse X-ray spectrometer. Prior to the analysis, samples were ground and homogenized in an agate mortar and glass discs were prepared by fusing about 0.3 g of bulk sediment with lithium tetraborate in an induction oven Perle'X-2. Analytical accuracy was checked by measuring international standards (GSS-1–GSS-7) and was better than 1% of certified values. Precision of individual measurements was better than 0.9% as determined from replicate analyses of sediment samples (repeatability). Precision over the period of measurement was better than 3.4% (reproducibility) for all elements analyzed in this work. In order to avoid spurious correlations between elements due to closure effect to 100%, i.e. dilution effects caused by variations in biogenic carbonate content (Wehausen and Brumsack, 2000), element/Al ratios (Rollinson, 1993) are discussed.

3.3. Grain-size analyses

Grain-size analyses were performed on both the *total fraction* (organic matter removed with 10% H₂O₂) and the *non-carbonate fraction* (both organic matter and carbonate were removed with H₂O₂ and HCl, respectively). Grain-size distributions were measured with a Coulter LS 100 laser particle size analyzer (CLS), which determines particle grain-sizes between 0.4 and 900 μm as volume percentages based on diffraction laws (McCave et al., 1986; Agrawal et al., 1991). Diffraction is assumed to be given by spherical particles and the particle size is given as an “equivalent spherical diameter”. Consequently, laser diffraction methods are claimed to underestimate plate-shaped clay mineral percentages. This underestimation has been corrected following Konert and Vandenberghe (1997). CLS precision and accuracy were tested by several control runs using latex micro-spheres with pre-defined diameters and the LS size control G15, which gave a coefficient of variation of 1.5%. Grain-size results are presented as the median of each sample since it represents the distribution midpoint and it usually constitutes a representative value of grain-size distribution better than the mean. In addition, the UP10 size (i.e. particles coarser than 10 μm) is considered, which adds the fine sand subpopulation to the sortable silt size fraction (10–63 μm) (McCave et al., 1995) and the silt/clay ratio as both parameters provide information about changes in paleocurrent intensity (Hall and McCave, 2000).

3.4. Chronostratigraphy

The age model for the upper 17 m of core MD99-2343 is based on 10 ¹⁴C-AMS datings covering the last 17 ka (Sierro et al., 2005; Frigola et al., 2007), the correlation of the *Globigerina bulloides* δ¹⁸O signal with the GISP2 oxygen isotopic record (Grootes et al., 1993; Meese et al., 1997) for MIS3 following (Sierro et al., 2005) and four additional tie points with the *G. bulloides* oxygen isotopic record from the Alboran Sea core MD95-2043 for the deglaciation and MIS2 (Cacho et al., 1999; Sierro et al., 2005) (Fig. 2 and Table 1). The ages were calibrated with the standard marine correction of 408 yr and the regional average marine reservoir correction (ΔR) for the western Mediterranean Sea by means of the Calib 5.0.1 program (Stuiver and Reimer, 1993) and the MARINE04 calibration curve (Hughen et al., 2004). Following this age model, which covers the last 50 kyr, the mean sedimentation rate for the top 17 m of core MD99-2343 is 36 cm kyr⁻¹ (Fig. 2), therefore allowing a centennial resolution in the study of the sediment record.

4. Results

4.1. Geochemical record

Several authors have used Si/Al, Ti/Al and K/Al ratios as proxies for terrigenous inputs in the Mediterranean region (Wehausen and Brumsack, 1999; Moreno et al., 2002; Weldeab et al., 2003; Frigola et al., 2007). Si mostly comes from aluminosilicates and quartz since biogenic opal is of minor importance in this sea due to its oligotrophic conditions and the dissolution of silica (Weldeab et al., 2003). Ti resides within heavy minerals such as ilmenite and rutile. K is associated with clay minerals, mainly illite (Wehausen and Brumsack, 1998, 2000).

Si/Al, Ti/Al and K/Al records from core MD99-2343 are shown in Fig. 3. The highly similar records of Si/Al and Ti/Al display a minimum from 13 to 10.5 ka that coincides with high summer insolation values (Fig. 3e). The decrease in the geochemical signal occurred during a pronounced decreasing trend of the oxygen isotopic signal from *G. bulloides* marking the last deglaciation (Frigola et al., 2007). The observed minima divides the Si/Al and Ti/Al records in to two parts: (i) from 50 to 13 ka, with high though variable values that characterize the glacial period, and (ii) from 10 ka to present time, with lower values and a smoother pattern. The last 10 kyr record, as described in detail in Frigola et al. (2007), can be divided into three successive phases: (i) an increasing phase in both ratios coincident with the end of the second phase of Termination (T1b) and the early Holocene (10.5–7 ka), (ii) a central plateau with relatively high values during the mid-Holocene (7–4 ka) and (iii) a gradually decreasing phase during the late Holocene (4–0 ka) (Fig. 3). The general long-term trend in the Si/Al and Ti/Al ratios is punctuated

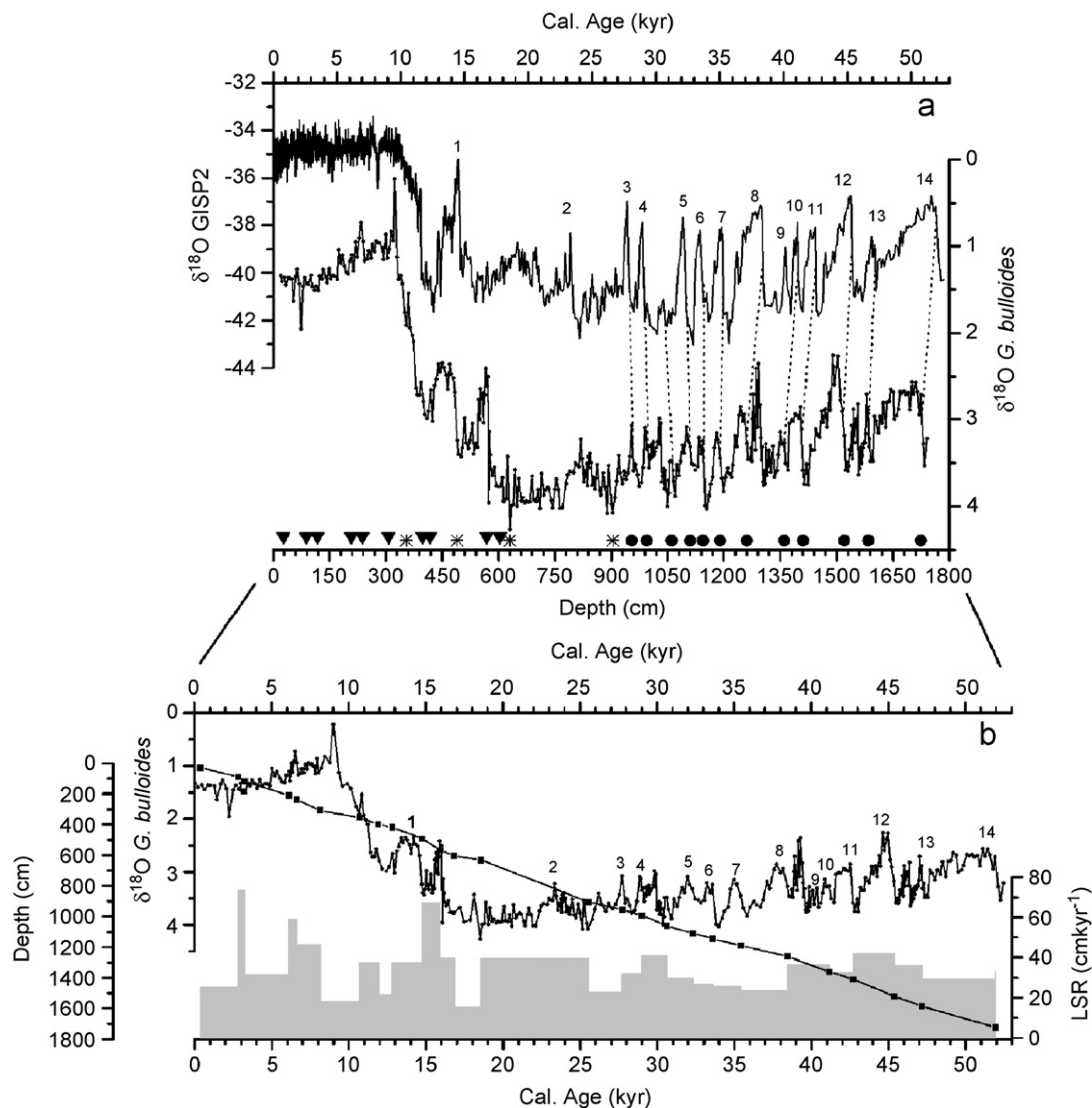


Fig. 2. (a) Age model of core MD99-2343 developed by means of 10^{14}C -AMS dates (triangles), the tuning of the *G. bulloides* $\delta^{18}\text{O}$ record with the ice $\delta^{18}\text{O}$ record from the GISP2 core (circles) and the tuning with the $\delta^{18}\text{O}$ record of the core MD95-2043 from the Alboran Sea (asterisks). See Table 1 for details. (b) Linear sedimentation rates (LSR) of core MD99-2343 for the last 50 kyr oscillating between 15 and 73 cm kyr^{-1} .

by eight abrupt relative increasing events coincident with increments in the planktonic $\delta^{18}\text{O}$ record. The general pattern of the K/Al record is completely different with its most remarkable feature being its high parallelism with the summer insolation curve at 40°N , which is particularly apparent for the last 40 kyr (Fig. 3d and e).

In addition to the observed general trends, geochemical ratios from core MD99-2343 exhibit pronounced millennial-scale changes during MIS3 that roughly correspond to the D–O oscillations described in the planktonic $\delta^{18}\text{O}$ record (Sierro et al., 2005), which parallel the Greenland Stadials (GSs) and Interstadials (GISs) from $\delta^{18}\text{O}$ ice records (Dansgaard et al., 1993; Grootes et al., 1993). That the geochemical and the isotopic records from core MD99-2343 are not completely in phase can be observed by comparing the plots in Fig. 3a–d. Abrupt increases of the geochemical ratios generally occur just after the lightest values of the $\delta^{18}\text{O}$ record have been reached coinciding

with the GIS/GS transitions. In contrast, the lowest Si/Al and Ti/Al values most often coincide with low values in the $\delta^{18}\text{O}$ record corresponding to GIS.

Five abrupt increases in Si/Al and Ti/Al ratios have been identified at 46, 39, 30, 24 and 16 ka that, with one exception, parallel the incursions of the polar water species *Neogloboquadrina pachyderma* (s) (Fig. 3f). These increases in the geochemical proxies also fit with peaks of abundance of the coccolithophore *Emiliania huxleyi* ($>4\ \mu\text{m}$) (Fig. 3g) (Sierro et al., 2005), which is identified as a cold water species indicator in NE Atlantic and Mediterranean regions (Colmenero-Hidalgo et al., 2002, 2004). These intervals correlate with HE1–HE5 described in the North Atlantic region (Heinrich, 1988; Bond et al., 1992; Broecker et al., 1992). Opposite to Si/Al and Ti/Al ratios, the K/Al record generally shows abrupt decreases during the HEs, which are especially pronounced during the latest part of HE5, HE4 and HE1 (Fig. 3d). The lowest values in

Table 1
Tie points used for the age model of core MD99-2343

| Radiocarbon sample or isotope event/foram type | Core depth (cm) | ¹⁴ C age (yr BP)/tie points tuned with | Calendar years |
|--|-----------------|---|----------------|
| AMS 14C/multispecific | 28 | 790 (±40) | 386±55 |
| AMS 14C/ <i>G. inflata</i> | 88 | 3110 (±30) | 2816±50 |
| AMS 14C/multispecific | 118 | 3390 (±50) | 3225±80 |
| AMS 14C/ <i>G. inflata</i> | 208 | 5720 (±40) | 6091±70 |
| AMS 14C/multispecific | 238 | 6210 (±50) | 6601±70 |
| AMS 14C/ <i>G. inflata</i> | 308 | 7700 (±40) | 8110±60 |
| Tib—Onset of the Holocene | 354 | MD95-2043 | 10,696 |
| AMS 14C/ <i>G. bulloides</i> | 398 | 10,650 (±50) | 11,883±230 |
| AMS 14C/ <i>G. inflata</i> | 418 | 11,200 (±50) | 12,811±30 |
| Base Bolling–Allerod | 490 | MD95-2043 | 14,750 |
| AMS 14C/ <i>G. bulloides</i> | 568 | 13,850 (±40) | 15,912 ±190 |
| AMS 14C/multispecific | 604 | 14,550 (±110) | 16,820 ±240 |
| LGM | 630 | MD95-2043 | 18,539 |
| Enrichment after Interstadial 3 | 904 | MD95-2043 | 25,525 |
| Base Interstadial 3 | 954 | GISP2 | 27,736 |
| Base Interstadial 4 | 994 | GISP2 | 29,000 |
| Base warming event | 1060 | GISP2 | 30,619 |
| Base Interstadial 5 | 1110 | GISP2 | 32,300 |
| Base Interstadial 6 | 1144 | GISP2 | 33,587 |
| Base Interstadial 7 | 1190 | GISP2 | 35,400 |
| Base Interstadial 8 | 1260 | GISP2 | 38,432 |
| Base Interstadial 10 | 1360 | GISP2 | 41,172 |
| Base Interstadial 11 | 1410 | GISP2 | 42,713 |
| Base Interstadial 12 | 1520 | GISP2 | 45,360 |
| Base Interstadial 13 | 1584 | GISP2 | 47,146 |
| Base Interstadial 14 | 1724 | GISP2 | 51,933 |

Ten ¹⁴C-AMS dates were calibrated with the Calib 5.0.1. program (Stuiver and Reimer, 1993) and the MARINE04 calibration curve (Hughen et al., 2004). Prior to 27 ka the age model is based on the correlation with the GISP2 ice core (Grootes et al., 1993; Meese et al., 1997). Four additional tie points were added through the comparison of the *G. bulloides* δ¹⁸O from both cores MD99-2343 and MD95-2043 (Cacho et al., 1999; Sierro et al., 2005). The age model was performed with the AnalySeries Version 1.1 (Paillard et al., 1996).

the K/Al record are the most recent ones that correspond to the current summer insolation minimum (Fig. 3d and e).

4.2. Grain-size record

Median grain-size values (between 4 and 9 μm) of both bulk and non-carbonate sediment fractions show fairly similar features (Fig. 4b) thus pointing to the same processes controlling the deposition of the two fractions. However, due to the mixed origin of the carbonate fraction (e.g. sea surface production of carbonate particles and inputs from the carbonate Balearic shelf), the non-carbonate fraction better represents the intensity of bottom currents (McCave et al., 1995).

The sortable silt size (10–63 μm) has been used as a proxy to infer the intensity of deep water currents (McCave et al., 1995). However, since strong contour currents are also able to rework particles coarser than 63 μm, the UP10 fraction has been considered here for the study of paleocurrent intensity (Frigola et al., 2007). The general trend from UP10 and silt/clay ratio profiles through the last 50 kyr shows affinities with the summer insolation record at 40°N (Fig. 4c–e). As for the geochemical proxies, grain-size records present different patterns during the glacial and interglacial periods, with a marked decreasing trend from

15 ka until 10.5 ka, which corresponds to the highest part of the rising limb of the summer insolation curve at 40°N. This reduction in the grain-size records is two-step and seems to show some relation with the two phases of the deglaciation interval marked by almost synchronous decreases in the *G. bulloides* δ¹⁸O profile (thus embracing the Younger Dryas). After the minimum grain-size values at 10.5 ka, relatively coarse grain-size values quickly resume at the onset of the Holocene. A general decreasing trend characterizes the last 9 kyr of the UP10 and silt/clay records that roughly parallel the *G. bulloides* δ¹⁸O increasing trend (Fig. 4a, c and d). This overall Holocene tendency towards grain-size reduction coincides with a diminution of the seasonal insolation differences at 40°N (Fig. 4e). Superimposed on the general long-term trend, the grain-size record is punctuated by eight abrupt increases known as Minorca abrupt events (Frigola et al., 2007).

The glacial period is characterized by mean higher and more variable grain-size values than the Holocene. From 50 to 29 ka background levels are punctuated by a series of millennial-scale oscillations at D–O cyclicities (Fig. 4c and d). It is worth to note that these records are not totally synchronous with the *G. bulloides* δ¹⁸O: low values of the grain-size proxies are coincident with low values in the δ¹⁸O record (GIS), while abrupt increases in the grain-size

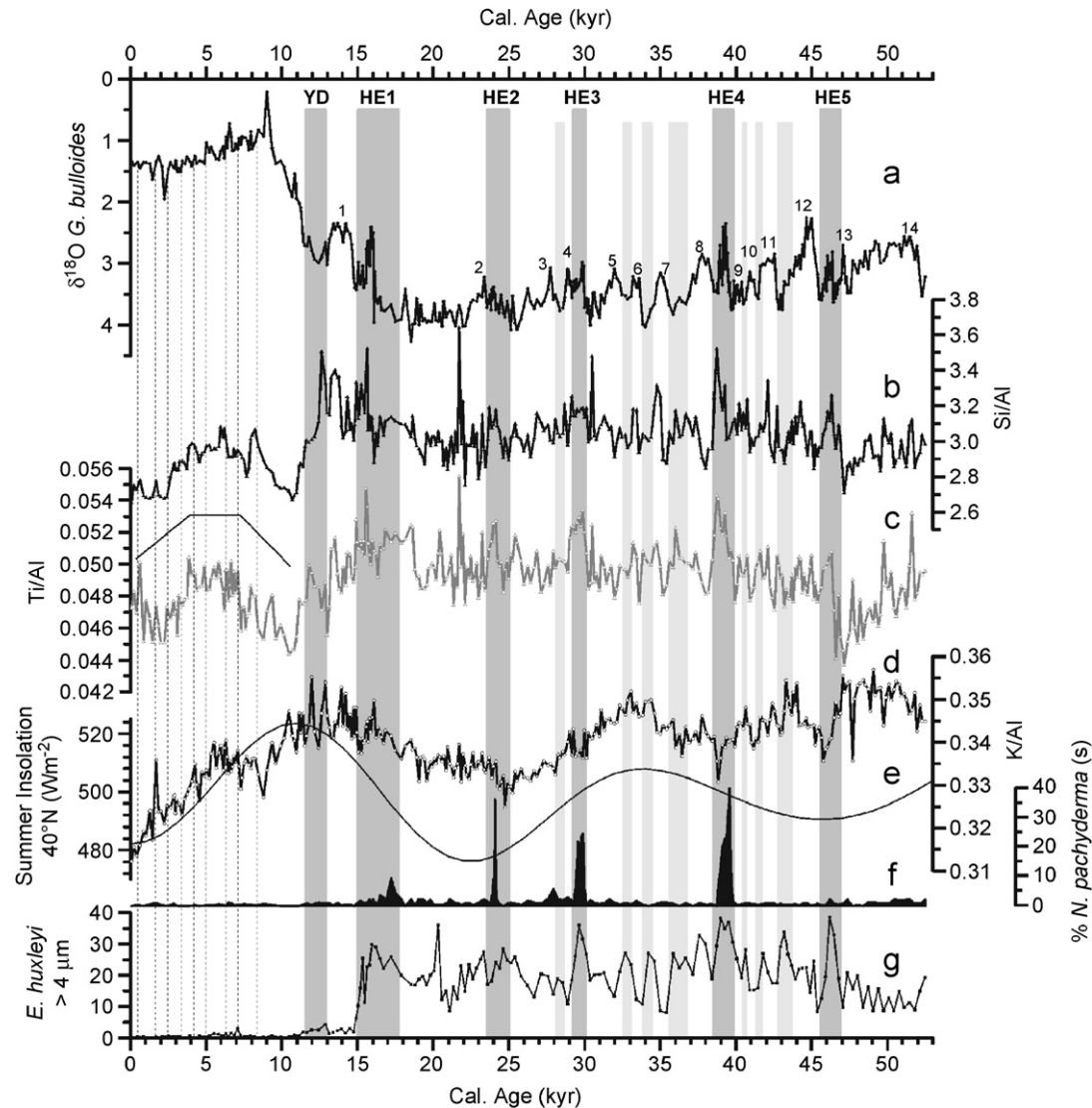


Fig. 3. (a) *G. bulloides* $\delta^{18}\text{O}$ record from core MD99-2343 for the last 50 kyr. Numbers above the curve represent warm GIS while gray bars correspond to cold GS, HEs and YD cold events. Vertical dashed lines to the left correspond to the Minorca abrupt events defined by Frigola et al. (2007) during the Holocene. (b, c and d) Si, Ti and K geochemical records normalized to Al, respectively. A continuous line between the Si/Al and the Ti/Al ratios embracing the 10.5–0 ka period represents three main phases within the general trend (see main text). (e) Summer insolation curve at 40°N for the last 50 kyr. (f) Percentages of polar water species *Neogloboquadrina pachyderma* (s). (g) Percentages of *E. huxleyi* larger than $4\ \mu\text{m}$.

proxies occur coincident with the GIS/GS transitions (Fig. 4a, c and d). In spite of the lack of synchrony among grain-size proxies and the planktonic $\delta^{18}\text{O}$ record, the pattern that characterizes a D–O cycle is very systematic. Increases in the silt/clay and in the UP10 fraction are abrupt while decreases are somewhat smoother, e.g. during GIS12 or GIS8, and almost parallel to the increasing trend observed in the $\delta^{18}\text{O}$ record from GIS to GS transitions (Fig. 4a, c and d). In addition, sudden increases in the silt/clay ratio also occur at the end of a series of abrupt progressively shorter oscillations, which are coincident with HE5, HE4 and HE3, identified from the *G. bulloides* $\delta^{18}\text{O}$ record (Sierra et al., 2005). The D–O variability in the grain-size proxies is interrupted by an abrupt decrease at 29–28 ka where very low values occur. This reduction in the grain-size proxies was contemporary with an important

decrease in the orbitally induced seasonal differences at times when winter insolation values were higher than at present (Fig. 4e). After that reduction a general increasing trend in both proxies from 26 to 15 ka is almost coincident with the increase in the summer insolation at 40°N or, in other words, with an increase in the orbitally induced seasonal differences (Fig. 4e).

5. Discussion

5.1. Orbitally-driven trends in the terrigenous signal

The K/Al record from core MD99-2343 shows a rather smooth pattern during the last 50 kyr that roughly parallels the summer insolation at 40°N with minimum values occurring during times of low summer insolation (Fig. 3).

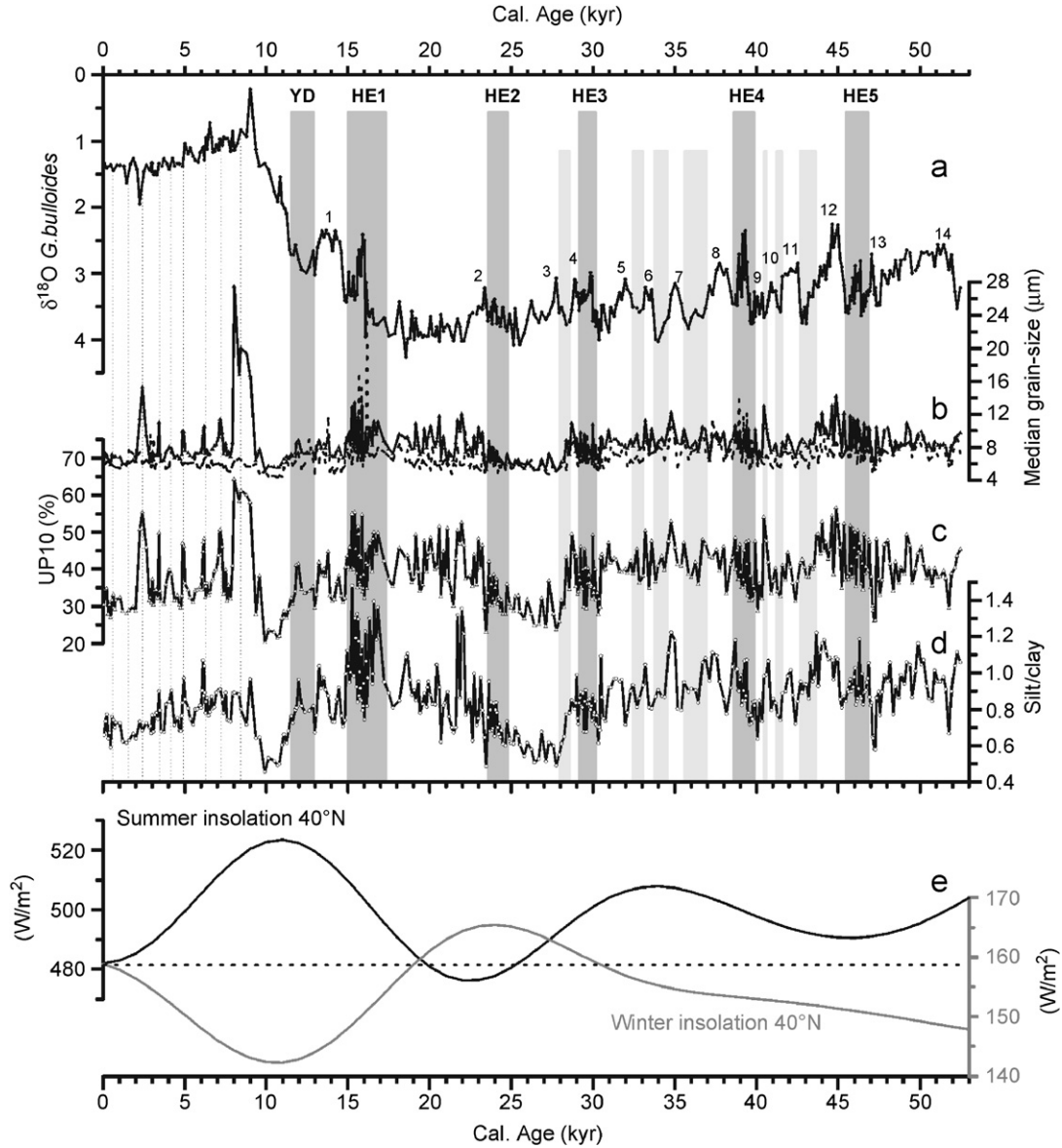


Fig. 4. (a) *G. bulloides* $\delta^{18}\text{O}$ record from MD99-2343 for the last 50 kyr. Numbers above the curve represent warm GIS while gray bars correspond to cold GS, HEs and YD cold events. Vertical dashed lines to the left correspond to the Holocene Minorca abrupt events defined by Frigola et al. (2007). (b) Median grain-size records of the total (dashed line) and non-carbonate sediment fractions (solid line). (c and d) UP10 fraction ($> 10\ \mu\text{m}$) and silt/clay ratio of the non-carbonate fraction, respectively. (e) Summer and winter insolation curves at 40°N for the last 50 kyr. Current values of both summer and winter insolation are plotted at the same level so that distances between both records through time can be interpreted as orbitally induced seasonal differences.

Superimposed on this long-term trend, millennial-scale oscillations appear as relatively minor features of the record. Sea level changes associated with the last deglaciation did not seem to produce any clear modulation in the K/Al record. These results suggest that K/Al oscillations have been mainly controlled by processes driven by orbitally induced insolation changes. Potassium (K) used to be mainly associated with clays, i.e. illite from continental runoff, and hence the K/Al ratio is interpreted in terms of river discharge (Wehausen and Brumsack, 1998, 2000). In the north-western Mediterranean region the Rhône and the Ebro rivers are the main sources of fluvial sediment inputs, with water supply mostly reflecting precipitation in the Alps and the Pyrenees, respectively.

Of these two main rivers, the Ebro clearly has a stronger Mediterranean character (i.e. a more pronounced seasonality). According to the MD99-2343 record, enhanced supply of clays (high K/Al values) occurred during periods of high summer insolation pointing to elevated precipitation or to a more efficient sediment transport regime, such as that produced due to increased torrential rains in general in the watersheds supplying the basin. In addition, enhanced aridification of the watersheds facilitates erosion resulting in higher lithogenic fluxes when seasonal rains occur (Fabres et al., 2002). These results indicate the strong control that orbitally induced insolation changes exerted on the fluvial runoff of detrital material in the western Mediterranean Basin at least during the last 50 kyr. In the

Eastern Mediterranean a precession control on Pliocene–Pleistocene sapropel formation and, therefore, on climatic and hydrographic conditions has been proposed by several authors (Hilgen, 1991; Rohling and Hilgen, 1991; Wehausen and Brumsack, 2000). The K/Al record from core MD99-2343 supports the precessional control on the climatic conditions of the western Mediterranean region as well.

Grain-size records, i.e. the silt/clay ratio, display a more complex pattern of variability. Although millennial-scale oscillations are very pronounced, a precessional frequency is also present, especially after 30 ka, when seasonal insolation differences are well marked (Fig. 4). Low silt/clay values occur during periods of relatively high winter insolation like the late Holocene and around 28 ka (Fig. 4d). Increments in the silt versus the clay fraction are attributed to enhanced deep currents able to transport coarse material to the Minorca sediment drift and winnow the finest sediment fraction. Deep water currents at the drift location belong to the WMDW mass whose overturning occurs in the Gulf of Lion. Formation of WMDW is a wintertime process and is strongly dependent on the intensity of north-westerly winds (MEDOC, 1970; Lacombe et al., 1985; Bethoux et al., 1990). The dominance of weaker deep currents at times of maximum winter insolation, as interpreted from the silt/clay ratio, is consistent with reduced intensities of the north-westerly winds during milder winters due to lower atmospheric pressure gradient and, consequently, with a less intense overturning in the Gulf of Lion.

This precessional-induced long-term pattern in the silt/clay ratio is sharply interrupted at 12–10 ka when winter insolation was at its minimum. Therefore, the silt/clay reduction occurred synchronously with the second phase of the Termination (T1b) suggesting that sea level oscillations also influenced deep water overturning in the basin. The low grain-size values recorded during this specific time interval are consistent with reduced deep water ventilation, which allowed the preservation of an organic rich layer (Cacho et al., 2002) and the dominance of low-oxygen benthic fauna (Caralp, 1988) in the Alboran Sea. Such a reduction in the western Mediterranean overturning further supports the effect of the post-glacial sea level rise on the stratification of Mediterranean waters during T1b, as suggested by former models (Rohling, 1994; Matthiesen and Haines, 2003). In addition, high K/Al values point to increased fluvial discharge because of more humid conditions at that time (Fig. 3d), which would also confirm persistent water column stratification. More humid conditions during the 12–10 ka interval have been also inferred from pollen and lacustrine sequences from the borderlands (Harrison and Digerfeldt, 1993; González-Sampériz et al., 2006). Overall, these results demonstrate that the combined effect of the post-glacial sea level rise (and the subsequent global reduction of the salinities of surface waters) and an astronomically induced precipitation increase enhanced water column stratification and, therefore, were responsible

for the reduction of the deep water overturning in the western Mediterranean. These mechanisms likely extended to the whole Mediterranean Basin and anticipated the formation of Sapropel 1 in the eastern Mediterranean Basin (Rohling, 1994).

Contrarily to the K/Al ratio, the Si/Al and Ti/Al records do not show consistent patterns of variability related to precessional insolation changes. Both Si/Al and Ti/Al ratios are associated with terrigenous inputs and should reflect changes in the processes controlling the amount and/or distribution of such inputs to the basin (Matthewson et al., 1995; Reichart et al., 1997; Wehausen and Brumsack, 2000; Moreno et al., 2002; Weldeab et al., 2003; Frigola et al., 2007). The observed differences between Si/Al, Ti/Al and K/Al ratios should be related to grain-size geochemical segregation since Si and Ti are related to coarse minerals and K to clay minerals. Consequently, Si/Al and Ti/Al ratios should be linked to processes controlling the grain-size distribution in the Minorca rise at higher frequencies than precessional. This interpretation is supported by the good correlation of these two geochemical ratios and the silt/clay ratio where most variability occurs at millennial time-scales.

5.2. Millennial-scale variability during the Holocene

The general pattern of the Si/Al and Ti/Al records during the Holocene, following their marked reduction during the last deglaciation (see Section 5.1 and Fig. 3b and c), can be subdivided into three phases. The first phase (10.5–7 ka) shows increasing values in both geochemical ratios but also embraces a sharp increase in the grain-size proxies (Figs. 3 and 4) indicating the recovery of the WMDW formation at the onset and early Holocene after the highest sea level rise rate was achieved (Fleming et al., 1998).

During the second phase (7–4 ka), which is synchronous with the end of the post-glacial sea level rise (Fleming et al., 1998), a sort of plateau is observed in the Si/Al and Ti/Al ratios (Fig. 3b and c). This mid-Holocene phase illustrates the high control that the sea level rise exerted on the overturning system in the Gulf of Lion. This was a period when the rather small range of variation of the geochemical proxies (Fig. 3) suggests no significant changes occurred in the fluvial supply to the basin neither in the overturning cell in the Gulf of Lion. By contrast, during the same interval, strong changes were reported worldwide (Steig, 1999) and, in particular, from the Mediterranean borderlands (COHMAP, 1988; Cheddadi et al., 1997; Prentice et al., 1998; Magny et al., 2002) and the North African region (Vernet and Faure, 2000) as associated with the end of the African Humid Period (deMenocal et al., 2000). Such a mid-Holocene climate variability is attributed to the reduction of seasonal insolation differences after 5.5 ka (Fig. 4e), which lead to an abrupt transition from humid to arid conditions in North Africa and in the western Mediterranean region. However, the Si/Al and Ti/Al records do not

seem to respond to those changes and only K/Al shows a clear reduction after that moment. The observed discrepancies between the various geochemical proxies suggest again different forcings: while Si/Al and Ti/Al mainly reflect changes in deep water currents, with a fluvial input modulation, K/Al mainly shows changes of humidity conditions on the borderlands. Therefore, the K/Al descending general trend after 5.5 ka is in phase with the end of the African Humid Period (deMenocal et al., 2000) and marks the establishment of drier conditions.

During the third phase (4–0 ka) the trends of the Si/Al and Ti/Al ratios point to an overall reduction of fluvial inputs likely due to the establishment of drier conditions and reduced precipitation. The overall continued rapid descent of the K/Al recorded also during the late Holocene confirms the reduction of fluvial inputs that parallel diminishing seasonal insolation differences (Figs. 3d and 4e). In addition, the rather subtle decreasing trend observed in the silt/clay ratio during the late Holocene (Fig. 4d) also points to a reduction of the overturning cell in the Gulf of Lion. Less intense deep water currents and reduced fluvial inputs would translate into an overall decreasing trend of the sedimentation rates as observed in Fig. 2b. A lower atmospheric pressure gradient due to the diminished seasonal insolation differences likely favored the establishment of drier conditions during the late Holocene (McDermott et al., 1999; Jalut et al., 2000; Magny et al., 2002). In addition, reduced north-westerly winds from a lowered pressure gradient system would be responsible for the lessening of deep water overturning and, consequently, for lower values in the silt/clay ratio (Fig. 4d).

Superimposed on the general Holocene trends, nine $\delta^{18}\text{O}$ incremental events with a periodicity close to 1000 yr relate to short cooling events, known as Minorca abrupt events (Fig. 3) (Frigola et al., 2007). Most of these events are characterized by parallel increases in the UP10 and in the Si/Al records (Figs. 3b and 4c) suggesting an intensification of the deep water currents intensity related to an enhancement in the Gulf of Lion's overturning system likely promoted by strengthened north-westerly winds. The timing of the Minorca abrupt events fits well with temperature oscillations from the Holocene $\delta^{18}\text{O}$ record in Greenland (Frigola et al., 2007) and suggests a coupled ocean–atmosphere teleconnection mechanism for climate variability transfer between high latitudes and the Mediterranean region. A similar pattern was proposed by Rohling et al. (2002) for the Aegean Sea in the eastern Mediterranean Sea. The occurrence of rapid climate cooling events during the Holocene has been reported worldwide (Mayewski et al., 2004) although disagreements about their precise timing, character and impact require more devoted research to understand the ultimate causes of these millennial-scale climate variability. Although insolation changes (Bond et al., 2001) and instabilities inherent to the North Atlantic THC (Schulz and Paul, 2002) have been proposed as the main causes of the Holocene climate

variability, the climatic oscillations recorded in the terrigenous signal of core MD99-2343 are better linked to the temperature signal from the North Atlantic region as highlighted by the correlation with the GISP2 $\delta^{18}\text{O}$ profile (Frigola et al., 2007). These results suggest that the atmospheric teleconnection between high latitudes and the Mediterranean region through the westerly winds system was the main control over the western Mediterranean deep circulation during the Holocene.

5.3. D–O variability in WMDW formation

Oxygen and carbon isotopic records from benthic foraminifera in cores MD99-2343 (Fig. 5) and MD95-2043, the later from the Alboran Sea, follow a pattern that is coherent with the D–O events (Cacho et al., 2000; Sierro et al., 2005). These oscillations have been interpreted in terms of changes in the ventilation rates and properties of the deep water masses indicating the dominance of well-ventilated, colder/saltier, WMDW during the GS in contrast to the GIS (Cacho et al., 2006). The increase of WMDW ventilation was suggested to be associated with the strengthening of the north-westerly winds in the Gulf of Lion during GS (Cacho et al., 2000; Sierro et al., 2005). Prevailing dry and cold conditions on land were observed along the same intervals (Allen et al., 1999; Combourieu Nebout et al., 2002; Sánchez Goñi et al., 2002). Thus, the increased WMDW formation during GS likely favored stronger deep-water currents, and hence deposition of coarser material in the Minorca sediment drift. However, maximum values in the paleocurrent intensity proxies are not recorded during the intervals of maximum ventilation according to benthic isotopes (maximum $\delta^{13}\text{C}$ values). In contrast, grain-size and geochemical increments occur slightly after the warmest phases of GIS (minimum planktonic $\delta^{18}\text{O}$ values), that is, during the recovering of deep water ventilation in parallel to the starting of the SST cooling phase (B. Martrat, personal communication) (see dotted lines in Fig. 5). This pattern is very consistent for all the GIS/GS cooling transitions and also in all three proxies for paleocurrents intensity (silt/clay, Si/Al and Ti/Al). All three records show synchronous peaks during GIS/GS transitions, which lead by several centuries the maximum ventilation conditions (Fig. 5b and c). These consistent but unexpected results reflect a dichotomy between proxies indicating water chemical properties (benthic and planktonic isotopes) and proxies of water physical properties (grain-size and sediment geochemical proxies). Such a pattern as found in the Minorca sediment drift indicates the high sensitivity of deep water conditions to changes in the properties of surface waters associated with GIS/GS transitions. Overall, these results suggest that the deep-water Minorca sediment drift is particularly sensitive to changes in the vertical position of the WMDW core. Considering that the drift extends from 2100 m to more than 2700 m of water depth, the WMDW core may only occasionally flow at the depth of core MD99-2343, that is,

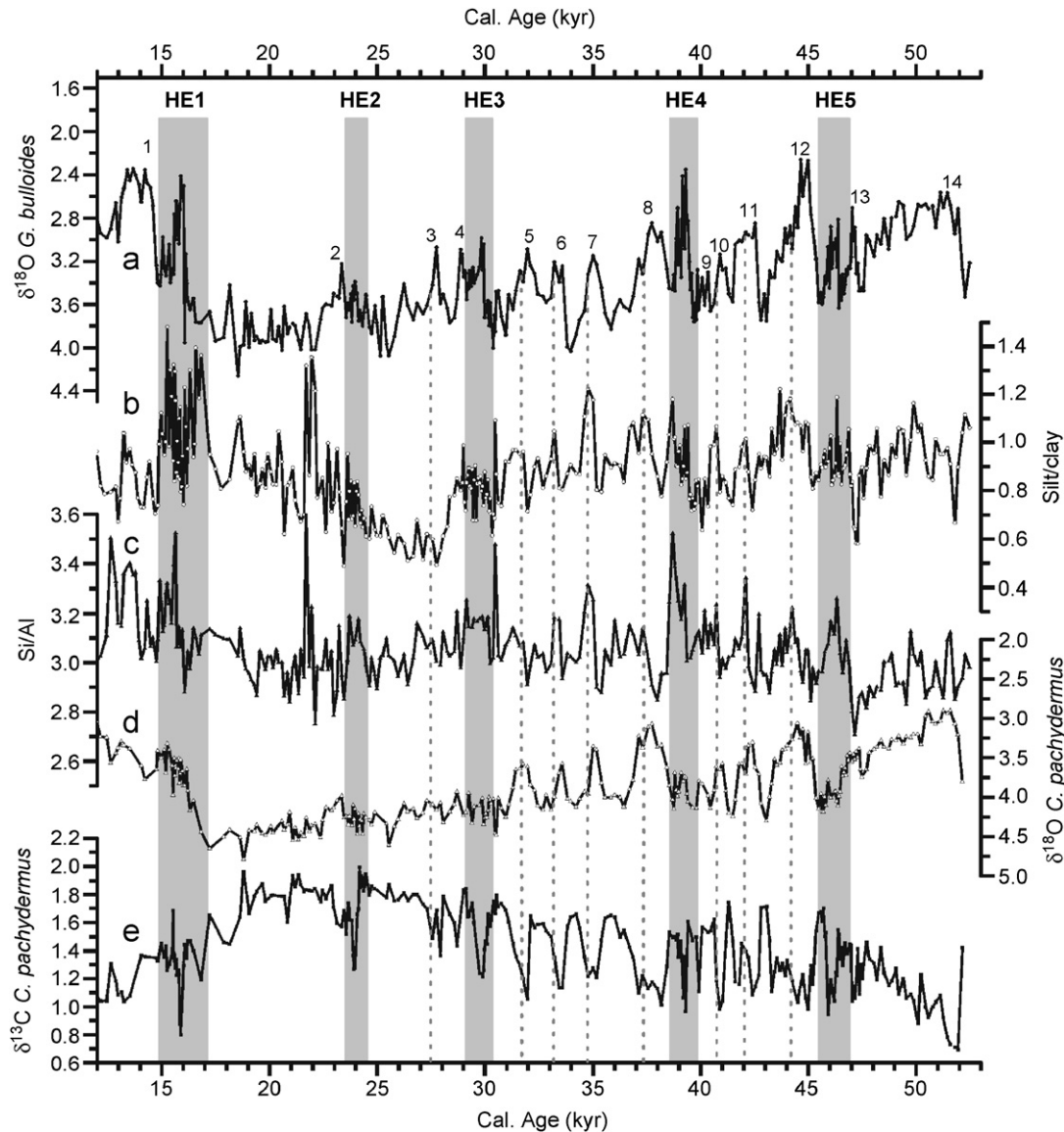


Fig. 5. Records from core MD99-2343 for the 12–50 ka time interval. (a) Planktonic $\delta^{18}\text{O}$. (b) Silt/clay ratio. (c) Si/Al. (d) Benthic $\delta^{18}\text{O}$. (e) Benthic $\delta^{13}\text{C}$. Numbers represent warm GIS while gray bars correspond to HEs. Dashed lines mark maximum values in the silt/clay ratio during MIS3.

2400 m. Therefore, paleointensity proxies indicate that GIS/GS transitions were the time when the WMDW core reached maximum strength at 2400 m. On the other hand, $\delta^{18}\text{O}$ and $\delta^{13}\text{C}$ records reflect chemical properties of the whole WMDW mass independently of the intensity and depth location of the flow core.

According to the patterns in the chemical and physical proxies along D–O cycles three main stages related to changes in WMDW properties can be defined (Fig. 6a). Stage 1 is a pure GIS stage with the lightest benthic and planktonic $\delta^{18}\text{O}$, light benthic $\delta^{13}\text{C}$ and low silt/clay values. Stage 2 corresponds to GIS/GS transitions, when SST cooled progressively, and benthic isotopes indicate improving ventilation (increasing $\delta^{13}\text{C}$) and incrementing density (increasing $\delta^{18}\text{O}$) of the WMDW. It is during Stage 2 when deep current speed proxies (i.e. silt/clay) indicate maximum velocities at the studied site. Stage 3 implies truly

GS conditions characterized by maximum $\delta^{18}\text{O}$ values in both planktonic and benthic foraminifera, maximum benthic $\delta^{13}\text{C}$ and intermediate values of the silt/clay ratio. Stages 1, 2 and 3 can be associated with a weak mode, an intermediate mode and a strong mode of deep-water overturning in the western Mediterranean Sea, respectively. These modes relate to GIS, GIS/GS transitions and GS situations.

Stage 1 corresponds then to intervals of minimum ventilation and lightest WMDW, which is consistent with the relatively warm and humid conditions on land during GISs (Combourieu Nebout et al., 2002; Sánchez Goñi et al., 2002) and minimum deep currents velocities at the MD99-2343 site. Stage 2 started after climate became gradually colder and drier, when the surface water cooling during GIS/GSs transitions likely resulted in an abrupt reduction of the water column density gradient thus

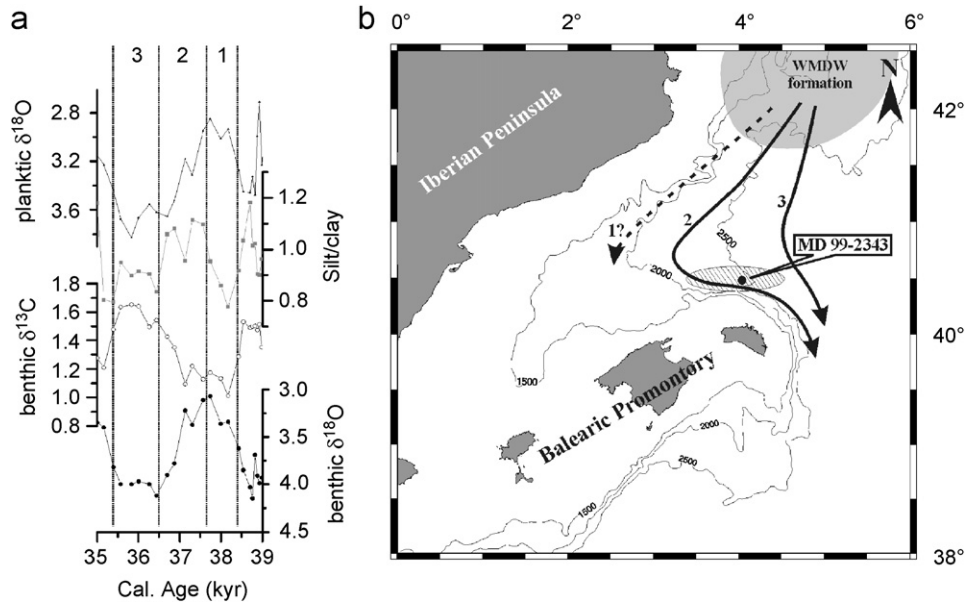


Fig. 6. (a) Detail of the planktonic $\delta^{18}\text{O}$, silt/clay, benthic $\delta^{13}\text{C}$ and benthic $\delta^{18}\text{O}$ records for the 35–39 ka time interval that corresponds to D–O cycle 8 (see Fig. 5). Numbers and vertical dotted lines limit the three stages described for each D–O cycle: Stage 1 during GIS, Stage 2 during GIS/GS transition and Stage 3 during GS. (b) Schematic bathymetric map showing the three modes of circulation within a D–O cycle. (1) weak mode, (2), intermediate mode and (3) strong mode. Depending on the properties of the WMDW formed in the Gulf of Lion (shaded area) the core of the deep currents circulates at different depths, thus having different effects on the Minorca sediment drift (striped area) where core MD99-2343 was recovered.

favoring reinforcement of deep water convection. Increased convection improved deep ventilation and resulted in maximum deep current velocities at the coring site as suggested by the highest silt/clay ratio (Figs. 5 and 6). During Stage 3, as surface conditions were becoming colder, the newly formed WMDW became progressively more ventilated and denser (increasing trends in $\delta^{13}\text{C}$ and $\delta^{18}\text{O}$) leading to a deepening of the bottom current core and, consequently, to a gradual speed reduction at the coring site as decreasing silt/clay ratio values suggest (Figs. 5 and 6). These results indicate that during times of maximum deep water formation (GS) the influence of the newly formed WMDW over the MD99-2343 site was reduced, likely due to a deeper circulation of those waters. Nevertheless, the silt/clay values recorded during Stage 3 suggest that currents were still active though to a lesser degree than at Stage 2 situations. The comparison among the benthic $\delta^{18}\text{O}$ and the grain-size records supports this hypothesis since current intensity systematically decreases when the heaviest $\delta^{18}\text{O}$ are reached (Fig. 5b and d). This observation is consistent with a new reconstruction of the properties of WMDW based on Mg/Ca paleothermometry in the Alboran Sea, which documents that the densest WMDW was formed during GS (Cacho et al., 2006). The recurrence of this pattern of variability with D–O cyclicity, with an offset between the physical proxies (e.g. silt/clay ratio) and the planktonic $\delta^{18}\text{O}$ record, demonstrates the extremely high sensitivity of the whole water column in the north-western Mediterranean Sea to climate-forced changes of surface water properties that modified the entire density gradient. Denser WMDW formed during GS changed the MOW density in a way that, during

intervals of denser MOW, the speed of its lower core increases as shown by coarsening mean grain-sizes from core MD99-2339 in the Gulf of Cadiz (Voelker et al., 2006).

The above described three modes of WMDW overturning appear as triggered by a rapid millennial-scale variability teleconnection between high and medium latitudes. Climate on land and intensity of westerly winds are the main forcing factors of present inter-annual variability in the intensity of WMDW formation together with the salt supply at intermediate levels from the eastern basin through the LIW (Lacombe et al., 1985; Schott and Leaman, 1991; Millot and Taupier-Letage, 2005). The westerlies intensity depends on the atmospheric pressure gradient over the North Atlantic region, in which decadal-scale variability presently is controlled by the NAO (Hurrell, 1995; Rodó et al., 1997). Assuming that a similar variability pattern acted during glacial times, it is likely that the observed changes in the WMDW circulation were controlled by NAO shifts. It has been already proposed that NAO oscillations dominated the glacial variability of the vegetation cover in the Iberian Peninsula and dust inputs from the Sahara region to the western Mediterranean Basin (Moreno et al., 2002; Sánchez Goñi et al., 2002). In addition, changes in the precipitation–evaporation budget at basin scale with D–O cyclicity have been inferred from pollen records in Italy, Greece and Iberia (Watts et al., 1996; Tzedakis, 1999; Sánchez Goñi et al., 2002). It is likely that these shifts in the precipitation–evaporation balance affected WMDW formation due to changes in surface salinity and, therefore, water density. These results also suggest that changes in the heat and salt

volumes exported through the MOW across the Strait of Gibraltar were associated with WMDW fluctuations and could have played an important feedback role in driving millennial-scale climate changes in the North Atlantic region (Bigg and Wadley, 2001).

5.4. Shifts in WMDW formation during HEs

The isotopic record during the GS associated with HEs shows a more complex pattern than the regular GS. Light benthic $\delta^{13}\text{C}$ events occur at the middle of these intervals in parallel with planktonic $\delta^{18}\text{O}$ depletions (Fig. 7). These surface anomalies would correspond to 2–4‰ salinity lowering caused by the entrance of fresher polar surface waters through the Strait of Gibraltar during each of the HEs (Cacho et al., 1999; Sierro et al., 2005). Such a surface freshening should have reinforced the water column stratification and opposed deep water convection in the Gulf of Lion (Sierro et al., 2005). Weak overturning during HE was not expected since extremely dry and cold conditions on land were reconstructed from pollen

sequences (Combourieu Nebout et al., 2002; Sánchez Goñi et al., 2002) and confirmed by the relatively low K/Al values recorded in MD99-2343 (Fig. 3d). Nevertheless, the benthic record indicates that, despite the climatic regime, the freshening of surface water was sufficient to reduce deep water formation (Sierro et al., 2005). Consequently, the GS associated with the HEs in the western Mediterranean had a complex deep ventilation evolution with high ventilation during the early and late phases (gray bars in Fig. 7) and a weakening in the middle of each HE due to surface water freshening (white bars in Fig. 7). All the proxies of deep water current speed (silt/clay, Si/Al and Ti/Al) show high values during the GS associated with the HEs which are consistent with the dominance of stronger deep currents by an active WMDW overturning (Figs. 3 and 4). These results are in contrast with the relatively low values recorded during the non-Heinrich GS and can only compare to the values recorded during GIS/GS transitions (stage 2 in Fig. 6).

The silt/clay record from the GS associated with the HEs does not show a clear systematic pattern of variability

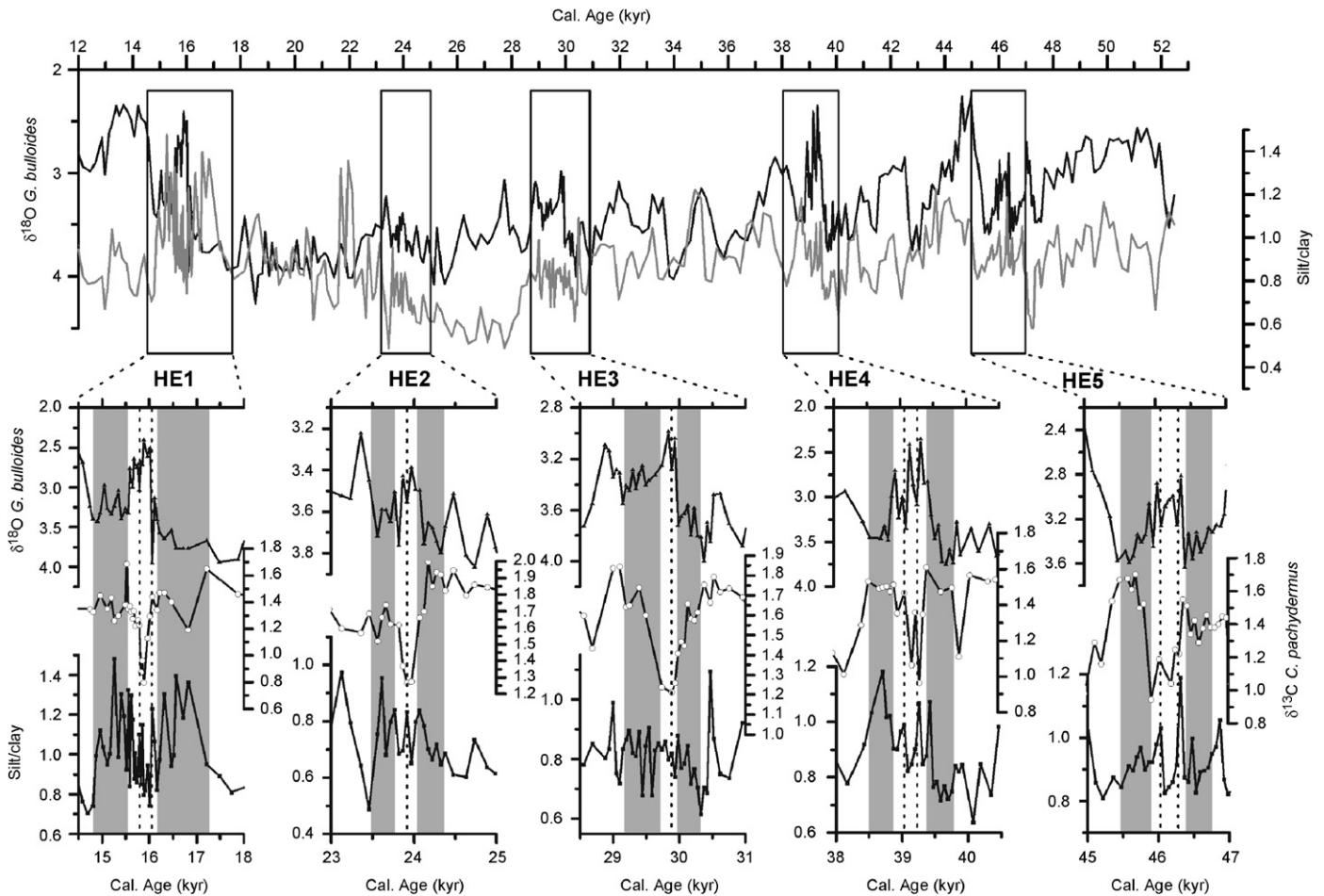


Fig. 7. Comparison of the planktonic $\delta^{18}\text{O}$ and the silt/clay ratio for the 12–50 ka time interval. A centuries long offset is observed among the silt/clay ratio and the planktonic $\delta^{18}\text{O}$ record during MIS3. Below, a close-up of HE1–HE5 through the planktonic $\delta^{18}\text{O}$, benthic $\delta^{13}\text{C}$ and silt/clay records from core MD99-2343 is shown. Gray bars represent the early and late phases of each HE while the white central bar corresponds to the isotopic anomaly described in the text. The high resolution reached on these records allows identification of several events in the central phase of each HE related to punctual returns to pure HE conditions (vertical dashed lines).

during the three phases described above. During HE1 and, to a lesser extent, during HE2 and HE4 lower silt/clay ratios are observed during the central phase (white bars in Fig. 7) compared to the early and late phases (gray bars). This pattern is clearly consistent with a weakening of the deep water current during the entrance of low-salinity polar waters. However, silt/clay values are comparable for all three phases during HE3 and HE5. These discrepancies in the pattern of each HE could be attributed to orbitally induced insolation changes, e.g. HE1 occurs in a period of increasing seasonal differences while HE3 occurs in a period of lessening seasonal differences (Fig. 4d and e).

The very high resolution of the silt/clay and isotopic records allows identifying additional minor structures within HEs (Fig. 7). In particular, during the surface freshwater anomaly (white bars in Fig. 7) one to two minor *G. bulloides* $\delta^{18}\text{O}$ increments are observed (dotted lines within white bars in Fig. 7). Most of them, i.e. those from HE5, HE4 and HE1, coincide with small *C. pachydermus* $\delta^{13}\text{C}$ increases. These minor recovering pulses are concurrent with marked increases in the silt/clay ratio, which supports the occurrence of deep currents short-lived strengthening events in the Minorca drift. These results suggest that the invasion of sub-polar less salty water from the North Atlantic was not steady but pulsating within each HE, which in turn triggered a response of the overturning cell in the Gulf of Lion. The combined interpretation of the isotopic and sedimentological records from core MD99-2343 suggests that, during GS associated with HEs, WMDW overturning was always strong enough to release fast currents to the Minorca drift, though not enough to reach the strongest mode 3 (Fig. 6) of non-Heinrich related GS. In consequence, sub-polar water pulses entering the western Mediterranean Basin induced changes in the intensity of WMDW ventilation but always allowed an intermediate mode of overturning.

6. Conclusions

The high-resolution sedimentological and geochemical analyses of the sediment core MD99-2343, recovered in the deep water Minorca sediment drift, resulted in new contributions to disentangle the variability of WMDW formation during the last 50 kyr. The strong parallelism between the K/Al record and the insolation curve at 40°N points to orbitally induced insolation changes as the main direct control over fluvial runoff in the western Mediterranean Basin, itself related to changes in the long-term precipitation pattern. This astronomical forcing also had an important effect on deep water formation in the western Mediterranean Basin as reflected by changes in the grain-size records from core MD99-2343, thus highlighting the strong climate sensitivity of the Mediterranean region to orbitally induced changes.

Millennial-scale oscillations from silt/clay, Si/Al and Ti/Al proxies paralleling oscillations in the isotopic records during MIS3 illustrate a pattern of high variability in the

deep water formation system in the western Mediterranean Basin that operates at three different intensity modes: strong, intermediate and weak. A centennial offset between the sedimentological and the isotopic proxies suggests that changes of intensity in deep water currents at MD99-2343 site resulted from density and paleodepth variations of the WMDW core flow thus affecting differently the Minorca sediment drift record. Since the formation of deep water during GIS was likely reduced, the cooling conditions prevailing after these warm events promoted the reduction of the column water density gradient thus favoring rapid reinforcement of deep water overturning and formation of denser WMDW that flowed into the deep basin. Accordingly, both silt/clay and Si/Al records from core MD99-2343 suggest maximum deep water currents intensity during the GIS/GS transitions, when WMDW core flowed shallower than the MD99-2343 site water depth. The continuous decreasing trend of silt/clay and Si/Al records until GS suggests a reduction of the effect of deep water currents at the core site location, thus pointing to the deepening of the WMDW core due to its increased density. On the other hand, silt/clay ratio centennial-scale oscillations recorded during HEs confirm the strong influence that the entrance of sub-polar low-salinity waters had on the overturning system in the Gulf of Lion and suggest the occurrence of fresh water pulses within each HE. The study of additional sequences from shallower and/or deeper water depths from the Minorca sediment drift is the only way to confirm or adjust the hypothesis of WMDW vertical shifts hypothesis during MIS3.

Furthermore, the grain-size and geochemical proxies from core MD99-2343 have shown to be very useful for the study of the deep water conditions in the western Mediterranean Basin providing the first Holocene reconstruction of WMDW variability in the absence of benthic foraminifera. The reduction observed in both grain-size and geochemical records during the 12–10 ka time interval corresponds to the slowing down or collapse of the deep water overturning system due to enlarged freshwater input during the last deglaciation. The general pattern followed by both grain-size and geochemical proxies during the Holocene suggests a transition from relatively high-energetic and humid conditions to drier conditions and less intense deep water currents. This transition was modulated by a reduction of the orbitally induced seasonal differences around 4 ka. Superimposed on this general trend, several rapid grain-size and geochemical excursions have been related to abrupt climate events. Thus, parallel increases in both the grain-size and geochemical records suggest a reinforcement of the deep water formation system coinciding with relative increases in the planktonic $\delta^{18}\text{O}$. The occurrence of such abrupt events during the Holocene at a periodicity close to 1000 yr and the good agreement with temperature oscillations in Greenland suggest a direct climatic teleconnection between the North Atlantic and the Mediterranean regions. The results from this work highlight the rapid response of the western Mediterranean

overturning system to changes in the properties of surface waters, indicating the rapid transmission of climate variability to the deep basin.

Acknowledgments

We are especially grateful to R/V *Marion Dufresne* crew and the IMAGES program that allowed collecting the core MD99-2343. We also thank Montse Guart and Elisenda Seguí for their help in the laboratory. This work has been supported by the European projects PROMESS 1 (EVR1-CT-2001-00041), EURODOM (RTN2-2001-00281), ADIOS (EVK3-2000-00604), EUROSTRATAFORM (EVK3-2001-00200) and HERMES (GOCE-CT-2005-511234-1). The Spanish funded CGL200500642/BTE, SA008C05 and REN2003-08642-C02-02 projects are equally acknowledged. COMER Foundation and I3P postdoctoral program (CSIC) are also acknowledged for their support to I. Cacho and A. Moreno, respectively. CRG Marine Geosciences is recognized within the *Generalitat de Catalunya* excellence research groups program (ref. 2005SGR 00152).

References

- Agrawal, Y.C., McCave, I.N., Riley, J.B., 1991. Laser diffraction size analysis. In: Syvitski, J.P.M. (Ed.), *Principles, Methods, and Application of Particle Size Analysis*. Cambridge University Press, Cambridge, pp. 119–129.
- Allen, J.R.M., Brandt, U., Brauer, A., Hubberten, H.W., Huntley, B., Keller, J., Michael, K., Mackensen, A., Mingram, J., Negendank, J.F.W., Nowaczyk, N.R., Oberhänsli, H., Watts, W.A., Wulf, S., Zolitschka, B., 1999. Rapid environmental changes in southern Europe during the last glacial period. *Nature* 400, 740–743.
- Alonso, B., Canals, M., Palanques, A., Rehault, J.P., 1995. A deep-sea channel in the Northwestern Mediterranean Sea: morphology and seismic structure of the Valencia channel and its surroundings. *Marine Geophysical Researches* 17, 469–484.
- Barry, R.G., Chorley, R.J., 1998. *Atmosphere, Weather and Climate*. Routledge, London, New York.
- Bartov, Y., Goldstein, S.L., Stein, M., Enzel, Y., 2003. Catastrophic arid episodes in the Eastern Mediterranean linked with the North Atlantic Heinrich events. *Geology* 31, 439–442.
- Bethoux, J.P., Gentili, B., Raunet, J., Tailliez, D., 1990. Warming trend in the western Mediterranean deep water. *Nature* 347, 660–662.
- Bigg, G., Wadley, M.R., 2001. Millennial-scale variability in the oceans: an ocean modelling view. *Journal of Quaternary Science* 16, 309–319.
- Bolle, H.-J., 2003. *Mediterranean Climate. Variability and trends*. Springer, Heidelberg.
- Bond, G., Heinrich, H., Broecker, W.S., Labeyrie, L., McManus, J., Andrews, J.T., Huon, S., Jantschik, R., Clasen, S., Simet, C., Tedesco, K., Klas, M., Bonani, G., Ivy, S., 1992. Evidence for massive discharges of icebergs into the North Atlantic ocean during the last glacial period. *Nature* 360, 245–249.
- Bond, G., Broecker, W.S., Johnsen, S.J., McManus, J., Labeyrie, L., Jouzel, J., Bonani, G., 1993. Correlations between climate records from North Atlantic sediments and Greenland ice. *Nature* 365, 143–147.
- Bond, G., Kromer, B., Beer, J., Muscheler, R., Evans, M., Showers, W., Hoffmann, S., Lotti-Bond, R., Hajdas, I., Bonani, G., 2001. Persistent solar influence on North Atlantic climate during the Holocene. *Science* 294, 2130–2136.
- Broecker, W.S., Bond, G., Klas, M., Clark, E., McManus, J., 1992. Origin of the North Atlantic's Heinrich events. *Climate Dynamics* 6, 265–273.
- Cacho, I., Grimalt, J.O., Pelejero, C., Canals, M., Sierro, F.J., Flores, J.A., Shackleton, N.J., 1999. Dansgaard-Oeschger and Heinrich event imprints in Alboran Sea temperatures. *Paleoceanography* 14, 698–705.
- Cacho, I., Grimalt, J.O., Sierro, F.J., Shackleton, N.J., Canals, M., 2000. Evidence for enhanced Mediterranean thermohaline circulation during rapid climatic coolings. *Earth and Planetary Science Letters* 183, 417–429.
- Cacho, I., Grimalt, J.O., Canals, M., Sbaiffi, L., Shackleton, N., Schönfeld, J., Zahn, R., 2001. Variability of the western Mediterranean Sea surface temperature during the last 25,000 years and its connection with the northern hemisphere climatic changes. *Paleoceanography* 16, 40–52.
- Cacho, I., Grimalt, J.O., Canals, M., 2002. Response of the Western Mediterranean Sea to rapid climate variability during the last 50,000 years: a molecular biomarker approach. *Journal of Marine Systems* 33–34, 253–272.
- Cacho, I., Shackleton, N., Elderfield, H., Sierro, F.J., Grimalt, J.O., 2006. Glacial rapid variability in deep-water temperature and $\delta^{18}\text{O}$ from the Western Mediterranean Sea. *Quaternary Science Reviews* 25, 3294–3311.
- Calafat, A.M., Casamor, J.L., Canals, M., Nyffeler, F., 1996. Distribución y composición elemental de la materia particulada en suspensión en el Mar Catalano-Balear. *Geogaceta* 20, 370–373.
- Canals, M., Puig, P., de Madron, X.D., Heussner, S., Palanques, A., Fabres, J., 2006. Flushing submarine canyons. *Nature* 444, 354–357.
- Caralp, M.H., 1988. Late Glacial to recent deep-sea benthic foraminifera from the Northeastern Atlantic (Cadiz Gulf) and Western Mediterranean (Alboran Sea): paleoceanographic results. *Marine Micropaleontology* 13, 265–289.
- Cheddadi, R., Yu, G., Guiot, J., Harrison, S.P., Prentice, I.C., 1997. The climate of Europe 6000 years ago. *Climate Dynamics* 13, 1–9.
- COHMAP, M., 1988. Climatic changes of the last 18,000 years: observations and model simulations. *Science* 241, 1043–1052.
- Colmenero-Hidalgo, E., Flores, J.-A., Sierro, F.J., 2002. Biometry of *Emiliania huxleyi* and its biostratigraphic significance in the Eastern North Atlantic Ocean and Western Mediterranean Sea in the last 20000 years. *Marine Micropaleontology* 46, 247–263.
- Colmenero-Hidalgo, E., Flores, J.-A., Sierro, F.J., Bárcena, M.A., Löwemark, L., Schönfeld, J., Grimalt, J.O., 2004. Ocean surface water response to short-term climate changes revealed by coccolithophores from the Gulf of Cadiz (NE Atlantic) and Alboran Sea (W Mediterranean). *Palaeogeography, Palaeoclimatology, Palaeoecology* 205, 317–336.
- Combouret, N., Turon, J.L., Zahn, R., Capotondi, L., Londeix, L., Pahnke, K., 2002. Enhanced aridity and atmospheric high-pressure stability over the western Mediterranean during the North Atlantic cold events of the past 50 k.y. *Geology* 30, 863–866.
- Dansgaard, W., Johnsen, S.J., Clausen, H.B., Dahl-Jensen, D., Gundestrup, N.S., Hammer, C.U., Hvidberg, C.S., Steffensen, J.P., Sveinbjörnsdóttir, A.E., Jouzel, J., Bond, G., 1993. Evidence for general instability of past climate from a 250-kyr ice-core record. *Nature* 364, 218–220.
- deMenocal, P., Ortiz, J., Guilderson, T., Adkins, J., Sarnthein, M., Baker, L., Yarusinsky, M., 2000. Abrupt onset and termination of the African Humid Period: rapid climate responses to gradual insolation forcing. *Quaternary Science Reviews* 19, 347–361.
- Fabres, J., Calafat, A., Sanchez-Vidal, A., Canals, M., Heussner, S., 2002. Composition and spatio-temporal variability of particle fluxes in the Western Alboran Gyre, Mediterranean Sea. *Journal of Marine Systems* 33,34, 431–456.
- Fleming, K., Johnston, P., Zwart, D., Yokoyama, Y., Lambeck, K., Chappell, J., 1998. Refining the eustatic sea-level curve since the Last Glacial Maximum using far- and intermediate-field sites. *Earth and Planetary Science Letters* 163, 327–342.
- Frigola, J., Moreno, A., Cacho, I., Canals, M., Sierro, F.J., Flores, J.A., Grimalt, J.O., Hodell, D.A., Curtis, J.H. 2007. Holocene climate

- variability in the western Mediterranean region from a deep water sediment record. *Paleoceanography*, 22, PA2209, doi:10.1029/2006PA001307.
- González-Sampériz, P., Valero-Garcés, B.L., Moreno, A., Jalut, G., García-Ruiz, J.M., Martí-Bono, C., Delgado-Huertas, A., Navas, A., Otto, T., Dedoubat, J.J., 2006. Climate variability in the Spanish Pyrenees during the last 30,000 yr revealed by the El Portalet sequence. *Quaternary Research* 66, 38–52.
- Grootes, P., Stuiver, M., White, J.W.C., Johnsen, S.J., Jouzel, J., 1993. Comparison of oxygen isotope records from the GISP2 and GRIP Greenland ice cores. *Nature* 366, 552–554.
- Hall, I.R., McCave, I.N., 2000. Palaeocurrent reconstruction, sediment and thorium focussing on the Iberian margin over the last 140 ka. *Earth and Planetary Science Letters* 178, 151–164.
- Harrison, S.P., Digerfeldt, G., 1993. European lakes as palaeohydrological and palaeoclimatic indicators. *Quaternary Science Reviews* 12, 233–248.
- Heinrich, H., 1988. Origin and consequences of cyclic ice rafting in the Northeast Atlantic Ocean during the past 130,000 years. *Quaternary Research* 29, 142–152.
- Hilgen, F.J., 1991. Astronomical calibration of Gauss to Matuyama sapropels in the Mediterranean and implication for the geomagnetic polarity time scale. *Earth and Planetary Science Letters* 104, 226–244.
- Hughen, K., Baillie, M., Bard, E., Bayliss, A., Beck, J., Bertrand, C., Blackwell, P., Buck, C., Burr, G., Cutler, K., Damon, P., Edwards, R., Fairbanks, R., Friedrich, M., Guilderson, T., Kromer, B., McCormac, F., Manning, S., Bronk Ramsey, C., Reimer, P., Reimer, R., Remmele, S., Southon, J., Stuiver, M., Talamo, S., Taylor, F., van der Plicht, J., Weyhenmeyer, C., 2004. Marine04 Marine radiocarbon age calibration, 26–0 ka BP. *Radiocarbon* 46, 1059–1086.
- Hurrell, J.W., 1995. Decadal trends in the North Atlantic Oscillation: regional temperatures and precipitation. *Science* 269, 676–679.
- Jalut, G., Esteban Amat, A., Bonnet, L., Gauquelin, T., Fontugne, M., 2000. Holocene climatic changes in the Western Mediterranean, from south-east France to south-east Spain. *Palaeogeography, Palaeoclimatology, Palaeoecology* 160, 255–290.
- Konert, M., Vandenberghe, J., 1997. Comparison of laser grain size analysis with pipette and sieve analysis: a solution for the underestimation of the clay fraction. *Sedimentology* 44, 523–535.
- Lacombe, H., Tchernia, P., Gamberoni, L., 1985. Variable bottom water in the Western Mediterranean Basin. *Progress in Oceanography* 14, 319–338.
- López-Jurado, J.L., González-Pola, C., Vélez-Belchí, P., 2005. Observation of an abrupt disruption of the long-term warming trend at the Balearic Sea, western Mediterranean Sea, in summer 2005. *Geophysical Research Letters* 32, doi:10.1029/2005GL024430.
- Magny, M., Miramont, C., Sivan, O., 2002. Assessment of the impact of climate and anthropogenic factors on Holocene Mediterranean vegetation in Europe on the basis of palaeohydrological records. *Palaeogeography, Palaeoclimatology, Palaeoecology* 186, 47–59.
- Maldonado, A., Got, H., Monaco, A., O'Connell, S., Mirabile, L., 1985a. Valencia Fan (Northwestern Mediterranean): distal deposition fan variant. *Marine Geology* 62, 295–319.
- Maldonado, A., Palanques, A., Alonso, B., Kastens, K.A., Nelson, C.H., O'Connell, S., Ryan, W.B.F., 1985b. Physiography and deposition on a distal deep-sea system: the Valencia Fan (Northwestern Mediterranean). *Geo-Marine Letters* 5, 157–164.
- Martin, J.-M., Elbaz-Poulichet, F., Guieu, C., Loyé-Pilot, M.-D., Han, G., 1989. River versus atmospheric input of material to the Mediterranean Sea: an overview. *Marine Chemistry* 28, 159–182.
- Martrat, B., Grimalt, J.O., Lopez-Martinez, C., Cacho, I., Sierro, F.J., Flores, J.A., Zahn, R., Canals, M., Curtis, J.H., Hodell, D.A., 2004. Abrupt temperature changes in the Western Mediterranean over the past 250,000 years. *Science* 306, 1762–1765.
- Matthewson, A.P., Shimmield, G.B., Kroon, D., Fallick, A.E., 1995. A 300 kyr high-resolution aridity record of the North African continent. *Paleoceanography* 10, 677–692.
- Matthiesen, S., Haines, K., 2003. A hydraulic box model study of the Mediterranean response to post-glacial sea-level rise. *Paleoceanography* 18(4), 1084, doi:10.1029/2003PA000880.
- Mauffret, A., Labarbarie, M., Montadert, L., 1982. Les affleurements de series sedimentaires pre-pliocenes dans le bassin Mediterranee nord-occidental. *Marine Geology* 45, 159–175.
- Mayewski, P.A., Rohling, E.E., Stager, J.C., Karlen, W., Maasch, K.A., Meeker, L.D., Meyerson, E.A., Gasse, F., van Kreveld, S., Holmgren, K., 2004. Holocene climate variability. *Quaternary Research* 62, 243–255.
- McCave, I.N., Bryant, R.J., Cook, H.F., Coughanowr, C.A., 1986. Evaluation of a laser-diffraction-size analyzer for use with natural sediments. *Journal of Sedimentary Research* 56, 561–564.
- McCave, I.N., Manighetti, B., Robinson, S.G., 1995. Sortable silt and fine sediment size/composition slicing: parameters for palaeocurrent speed and palaeoceanography. *Paleoceanography* 10, 593–610.
- McDermott, F., Frisia, S., Huang, Y., Longinelli, A., Spiro, B., Heaton, T.H.E., Hawkesworth, C.J., Borsato, A., Keppens, E., Fairchild, I.J., 1999. Holocene climate variability in Europe: evidence from $\delta^{18}\text{O}$, textural and extension-rate variations in three speleothems. *Quaternary Science Reviews* 18, 1021–1038.
- MEDOC, G., 1970. Observation of formation of deep water in the Mediterranean Sea, 1969. *Nature* 227, 1037–1040.
- Meese, D.A., Gow, A.J., Alley, R.B., Zielinski, P.M., Grootes, G.A., Ram, M., Taylor, K.C., Mayewski, P.A., Bolzan, J.F., 1997. The Greenland ice sheet project 2 depth–age scale: methods and results. *Journal of Geophysical Research* 102, 26411–26423.
- Millot, C., 1999. Circulation in the Western Mediterranean Sea. *Journal of Marine Systems* 20, 423–442.
- Millot, C., Taupier-Letage, I., 2005. Circulation in the Mediterranean Sea. In: *The Handbook of Environmental Chemistry*. Springer, Berlin, Heidelberg, pp. 29–66.
- Moreno, A., Cacho, I., Canals, M., Prins, M.A., Sanchez-Goni, M.-F., Grimalt, J.O., Weltje, G.J., 2002. Saharan dust transport and high-latitude glacial climatic variability: the Alboran Sea record. *Quaternary Research* 58, 318–328.
- Moreno, A., Cacho, I., Canals, M., Grimalt, J.O., Sanchez-Vidal, A., 2004. Millennial-scale variability in the productivity signal from the Alboran Sea record, Western Mediterranean Sea. *Palaeogeography, Palaeoclimatology, Palaeoecology* 211, 205–219.
- Nelson, C.H., Maldonado, A., 1990. Factors controlling late Cenozoic continental margin growth from the Ebro Delta to the western Mediterranean deep sea. *Marine Geology* 95, 419–440.
- Paillard, D., Labeyrie, L., Yiou, P., 1996. Macintosh program performs time-series analysis. *Eos Transactions, American Geographical Union* 77, 379.
- Palanques, A., Kenyon, N.H., Alonso, B., Limonov, A., 1995. Erosional and depositional patterns in the Valencia channel mouth: an example of a modern channel-lobe transition zone. *Marine Geophysical Researches* 17, 503–517.
- Pinardi, N., Masetti, E., 2000. Variability of the large scale general circulation of the Mediterranean Sea from observations and modelling: a review. *Palaeogeography, Palaeoclimatology, Palaeoecology* 158, 153–173.
- Prentice, I.C., Harrison, S.P., Jolly, D., Guiot, J., 1998. The climate and biomes of Europe at 6000 yr BP: comparison of model simulations and pollen-based reconstructions. *Quaternary Science Reviews* 17, 659–668.
- Reichert, G.J., den Dulk, M., Visser, H.J., van der Weijden, C.H., Zachariasse, W.J., 1997. A 225 kyr record of dust supply, paleoproductivity and the oxygen minimum zone from the Murray Ridge (northern Arabian Sea). *Palaeogeography, Palaeoclimatology, Palaeoecology* 134, 149–169.
- Rodó, X., Baert, E., Comin, F.A., 1997. Variations in seasonal rainfall in northern Europe during the present century: relationships with the North Atlantic oscillation and the El Niño-southern oscillation. *Climate Dynamics* 13, 275–284.
- Rogerson, M., Rohling, E.J., Weaver, P.P.E., 2006. Promotion of meridional overturning by Mediterranean-derived salt during the last deglaciation. *Paleoceanography* 21, PA4101, doi:10.1029/2006PA001306.

- Rohling, E.J., 1994. Review and new aspects concerning the formation of eastern Mediterranean sapropels. *Marine Geology* 122, 1–28.
- Rohling, E.J., Hilgen, F.J., 1991. The eastern Mediterranean climate at times of sapropel formation: a review. *Geologie en Mijnbouw* 70, 253–264.
- Rohling, E.J., Hayes, A., Rijk, D., Kroon, D., Zachariasse, W.J., Eisma, D., 1998. Abrupt cold spells in the northwest Mediterranean. *Paleoceanography* 13, 316–322.
- Rohling, E.J., Mayewski, P.A., Abu-Zied, R.H., Casford, J.S.L., Hayes, A., 2002. Holocene atmosphere–ocean interactions: records from Greenland and the Aegean Sea. *Climate Dynamics* 18, 587–593.
- Rollinson, H., 1993. *Using Geochemical Data. Evaluation, Presentation, Interpretation*. Longman Scientific and Technical, New York.
- Sánchez Goñi, M.F., Cacho, I., Turon, J.-L., Guiot, J., Sierro, F.J., Peyrouquet, J.-P., Grimalt, J.O., Shackleton, N.J., 2002. Synchronicity between marine and terrestrial responses to millennial scale climatic variability during the last glacial period in the Mediterranean region. *Climate Dynamics* 19, 95–105.
- Schott, F., Leaman, K.D., 1991. Observations with moored acoustic doppler current profiles in the convection regime in the Gulf of Lion. *Journal of Physical Oceanography* 13, 316–322.
- Schulz, M., Paul, A., 2002. Holocene climate variability on centennial-to-millennial time scales: 1. Climate records from the North-Atlantic realm. In: Wefer, G., Berger, W., Behre, K.-E., Jansen, E. (Eds.), *Climate Development and History of the North Atlantic Realm*. Springer, Berlin, Heidelberg, pp. 41–54.
- Sierro, F.J., Hodell, D.A., Curtis, J.H., Flores, J.A., Reguera, I., Colmenero-Hidalgo, E., Bárcena, M.A., Grimalt, J.O., Cacho, I., Frigola, J., Canals, M., 2005. Impact of iceberg melting on Mediterranean thermohaline circulation during Heinrich events. *Paleoceanography* 20, PA2019, doi:10.1029/2004PA001051.
- Steig, E.J., 1999. Mid-Holocene climate change. *Science* 286, 1485–1487.
- Stocker, T.F., 2000. Past and future reorganizations in the climate system. *Quaternary Science Reviews* 19, 301–319.
- Stuiver, M., Reimer, P.J., 1993. Extended ^{14}C database and revised CALIB radiocarbon calibration program. *Radiocarbon* 35, 215–230.
- Tzedakis, P.C., 1999. The last climatic cycle at Kopais, central Greece. *Journal of the Geological Society, London* 156, 425–434.
- Velasco, J.P.B., Baraza, J., Canals, M., 1996. La depresión periférica y el lomo contourítico de Menorca: evidencias de la actividad de corrientes de fondo al N del Talud Balear. *Geogaceta* 20, 359–362.
- Vernet, R., Faure, H., 2000. Isotopic chronology of the Sahara and the Sahel during the late Pleistocene and the early and Mid-Holocene (15,000–6,000 BP). *Quaternary International* 68–71, 385–387.
- Voelker, A.H.L., Lebreiro, S.M., Schonfeld, J., Cacho, I., Erlenkeuser, H., Abrantes, F., 2006. Mediterranean outflow strengthening during northern hemisphere coolings: a salt source for the glacial Atlantic? *Earth and Planetary Science Letters* 245, 39–55.
- Watts, W.A., Allen, J.R.M., Huntley, B., 1996. Vegetation history and palaeoclimate of the last glacial period of Lago Grande di Monticchio, southern Italy. *Quaternary Science Reviews* 15, 133–153.
- Wehausen, R., Brumsack, H.-J., 1998. The formation of Pliocene Mediterranean sapropels: constraints from high-resolution major and minor element studies. In: Robertson, A.H.F., Emeis, K.-C., Ritcher, C., Camerlenghi, A. (Eds.), *Proceedings of the Ocean Drilling Program, Scientific Results*, pp. 207–217.
- Wehausen, R., Brumsack, H.-J., 1999. Cyclic variations in the chemical composition of eastern Mediterranean Pliocene sediments: a key for understanding sapropel formation. *Marine Geology* 153, 161–176.
- Wehausen, R., Brumsack, H.-J., 2000. Chemical cycles in Pliocene sapropel-bearing and sapropel-barren eastern Mediterranean sediments. *Palaeogeography, Palaeoclimatology, Palaeoecology* 158, 325–352.
- Weldeab, S., Siebel, W., Wehausen, R., Emeis, K.-C., Schmiedl, G., Hemleben, C., 2003. Late Pleistocene sedimentation in the Western Mediterranean Sea: implications for productivity changes and climatic conditions in the catchment areas. *Palaeogeography, Palaeoclimatology, Palaeoecology* 190, 121–137.